Computers and Geotechnics 138 (2021) 104317

Contents lists available at ScienceDirect

Computers and Geotechnics

journal homepage: www.elsevier.com/locate/compgeo

Numerical study of fractured rock masses: Transverse isotropy vs. implicit joint-continuum models

Hosung Shin [a,*], J. Carlos Santamarina [b]

[a] Dept. of Civil and Environmental Eng., University of Ulsan, South Korea
[b] Earth Science and Engineering, KAUST, Saudi Arabia

ARTICLE INFO

Keywords:
Fractured rock mass
Strip footing
Implicit joint-continuum model
Transverse isotropic model
FEM

ABSTRACT

Fractures prevail mechanical behavior of a rock mass and confer an overall anisotropic response. Engineering analyses in the elastic regime often use transverse isotropy to model fractured rock masses with a single fracture set. An alternative implicit joint-continuum model combines the mechanical response of the intact rock and fractures by adding their compliance matrices. It can accommodate multiple fracture sets and non-linear fracture response. While the transverse isotropic model is inadequate to model fractured rock media because of its inherent assumptions on the continuity for all stress components, the implicit joint-continuum model is verified against the exact solutions of internal stress distributions and displacement field. The analysis of strip foundations using the implicit joint continuum approach shows that the maximum settlement and tilt will take place when the fracture set strikes quasi-collinear with the strip direction ($\theta^J \approx \pm 15^\circ$) and the fracture dip angle is either $\beta^J \approx 40^\circ \pm 10^\circ$ or $\beta^J \approx 140^\circ \pm 10^\circ$.

1. Introduction

Discontinuities in rock masses range from bedding planes to fissures, fractures, and faults. The general term 'fracture' in this manuscript refers to geological discontinuities. Fractures have higher mechanical compliance and hydraulic permeability than the surrounding intact rock (Cai and Horii, 1992; Oda et al., 1993) and impart an anisotropic hydraulic and mechanical response. Rock mass ratings consider fracture characteristics to inform the engineering analysis of slopes, foundations, and tunnels with the rating adjustment (Bieniawski, 1973; Bindlish et al., 2012).

The design of foundations subjected to high loads such as high-rise buildings, arch dams, and large bridges demands careful consideration of the rock mass properties (Hungr and Coates, 1978; Serrano and Olalla, 1996). The prediction of displacement and stress fields beneath shallow foundations resting on fractured rock masses is challenging even for the simplest case in two-dimensional analyses (Alehossein et al., 1992; Davis, 1980; Imani et al., 2012; Maghous et al., 2008; Prakoso and Kulhawy, 2004; Sutcliffe et al., 2003; Zhang et al., 2012; Yu, 2006). Due to the inherent difficulties in large-scale field tests, bearing capacity is generally estimated by rock core tests and empirical corrections related to the rock mass rating disregarding joint orientation. Its assessment is also available from analytical and numerical methods such as limit analysis, slip line, block/wedge analyses, or finite elements (Imani et al., 2012; Prakoso and Kulhawy, 2004; Sutcliffe et al., 2003; Zhang and Lei, 2014). Settlement analyses are equally challenging when fractured rock masses are involved. There are some solutions for cross anisotropic media, such as radial stress distribution beneath a line load for varying joint orientation (assumes no shear stress – Bray, 1977), and stress and deformation fields when the load direction is collinear with the direction of anisotropy in transverse isotropy (Bell, 1992; Duncan and Christopher, 2005; Gerrard and Harrison, 1970; Liao and Wang, 1998; Wang et al., 2006).

Despite advances in numerical and analytical techniques, satisfactory modeling remains difficult and uncertain (Jing, 2003). This manuscript documents a study of shallow foundations on fractured rock masses. It explore limitations in the inclined transverse isotropy model and compare results against the recently developed implicit joint-continuum model (Shin and Santamarina, 2019).

2. Numerical models for fractured rock mass

This section reviews the formulation for the transverse isotropic model, followed by a brief description of the implicit join-continuum

* Corresponding author.
E-mail address: shingeo@ulsan.ac.kr (H. Shin).

https://doi.org/10.1016/j.compgeo.2021.104317
Received 24 May 2020; Received in revised form 17 June 2021; Accepted 18 June 2021
Available online 26 June 2021

model.

2.1. Inclined transverse isotropic model

Transverse isotropy is the simplest model that can represent the anisotropic behavior of a rock mass. The model is well suited for layered rocks and rock masses with a single fracture set where the rock is isotropic within the plane of symmetry (Amadei and Goodman, 1981; Cho et al., 2012).

Transverse isotropy (local coordinate system xyz where z is normal to the isotropic plane). Five elastic constants describe transverse anisotropy: stiffness and Poisson's ratio E_p and $\nu_p = \nu_x = \nu_y$ on the isotropic xy-plane, E_z and ν_{zp} normal to the isotropic plane, and the shear modulus G_{zp} within the plane normal to the isotropic plane. The stiffness tensor is positive definite and enforces $\nu_{pz}E_z = \nu_{zp}E_p$. Consider a rock mass with a single fracture set normal to the z-axis and characterized by spacing s, normal fracture stiffness K_n, [Pa/m], and shear stiffness K_s [Pa/m]. The equivalent modulus E_z for the rock mass considers the intact rock in series with fractures (Goodman, 1989),

$$E_z^{-1} = E_p^{-1} + (s{\cdot}K_n)^{-1},\ G_{zp}^{-1} = G_p^{-1} + (s{\cdot}K_s)^{-1},\ \nu_{pz} = \nu_p \tag{1}$$

The elastic compliance matrix built with these five elastic constants gives the stress-strain relationship for the transverse isotropic material, $d\underline{\sigma} = D : d\underline{\varepsilon}$ (Hudson and Harrison, 2000).

Fracture plane in the global coordinate system XYZ. Three unit vectors define the fracture plane in the global coordinate system XYZ in terms of the fracture strike θ and dip β angles (Fig. 1).

$$\begin{array}{cc} \underline{n}_1 = (cos\theta{\cdot}cos\beta, -sin\theta{\cdot}cos\beta, -sin\beta) & \text{dip direction} \\ \underline{n}_2 = (sin\theta, cos\theta, 0) & \text{strike direction} \\ \underline{n}_3 = (cos\theta{\cdot}sin\beta, -sin\theta{\cdot}sin\beta, cos\beta) & \text{normal direction} \end{array} \tag{2}$$

In the definition of the fracture plane n_{ij}, the first sub-index (i) refers to the dip($i = 1$), strike($i = 2$) and normal($i = 3$) vectors, and the second sub-index (j) indicates 3 spatial components for the each direction vector.

Inclined transverse isotropy. These unit vectors define the rotation of the stiffness tensor D_{ijkl} from the fracture local coordinate system xyz onto the global coordinate system XYZ

$$D_{ijkl} = n_{pi}n_{qj}n_{rk}n_{sl}D_{pqrs} \tag{3}$$

where sub-indexes (i,j,k,l) are indexes of global coordinates, and sub-indexes (p,q,r,s) are the summation indexes used in the local stiffness tensor D_{pqrs}.

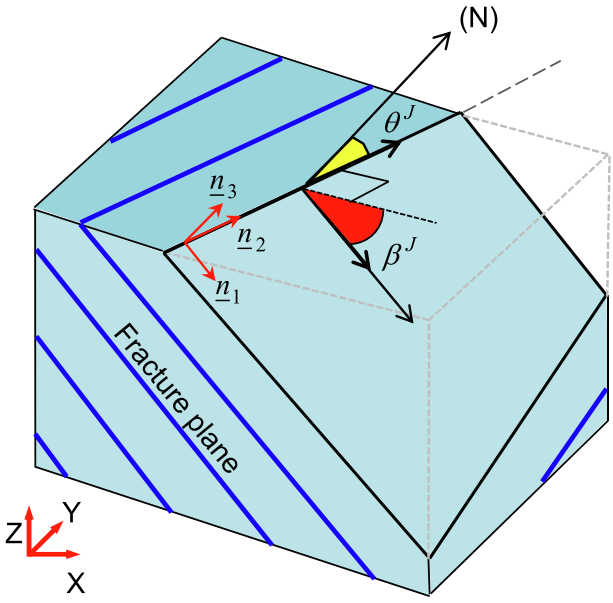

Fig. 1. Coordinate system and joint orientation.

Similarly, stresses in the global coordinate system are:

$$\sigma_{ij} = n_{ip}n_{jq}\sigma_{pq} \tag{4}$$

The inclined transverse isotropic model can efficiently capture the anisotropic mechanical behavior of a rock mass with a single fracture set only. Furthermore, it does not evaluate fracture displacements (elastic or plastic), and it cannot adequately capture fluid coupling. The implicit joint-continuum model described next overcomes these limitations.

2.2. Implicit joint-continuum model

A change in stress causes concurrent deformations in the intact rock and on fracture planes (Formulation details in Shin and Santamarina, 2019). The overall strain in the rock mass $\underline{\varepsilon}$ is the sum of the strain in the intact rock $\underline{\varepsilon}^C$ and the equivalent strain in fracture sets $\underline{\varepsilon}^J$ (Superscript C and J stand for intact continuum and the joint). The rock mass stiffness tensor relates the strain increment to the stress increment $d\underline{\sigma} = D^m d\underline{\varepsilon}$.

The mechanical behavior of a fractured rock mass satisfies stress continuity across fractures, and combines in series the stiffness of the intact rock and the equivalent stiffness of fractures. If compliance C is defined as the inverse of stiffness D, the equivalent compliance tensor for a fractured rock mass C^m is a linear summation of the compliance tensors of the intact rock C^C and each fracture set C^J.

$$C^m = C^C + \sum C^J \tag{5}$$

The compliance tensor for a single fracture set C^J is a 4th order tensor C^J_{ijkl}. It adds the compliances in each global direction (Shin and Santamarina, 2019),

$$\varepsilon^J_{ij} = C^J_{ijkl}\,\sigma_{kl} = \sum_r \frac{n_{3r}}{4{\cdot}s}\left(n_{pi}\delta_{rj} + n_{pj}\delta_{ri}\right){\cdot}c^J_{pq}{\cdot}n_{3r}{\cdot}\left(n_{qk}{\cdot}\delta_{rl} + n_{qi}{\cdot}\delta_{rk}\right){\cdot}\sigma_{kl} \tag{6}$$

where δ_{ij} is Kronecker's delta. The fracture stiffness matrix d^J_{pq} expresses the fracture elastoplastic stress-displacement response $S_p = d^J_{pq}{\cdot}u_q$ at the fracture scale, and it is used to compute the fracture compliance matrix $c^J_{pq} = \left[d^J_{pq}\right]^{-1}$.

At the scale of the rock mass, the compliance tensors of the intact rock C^C and of each fracture set C^J provide the strain components contributed by the intact rock $\underline{\varepsilon}^C$ and the fracture sets $\underline{\varepsilon}^J$ due to the applied stress $\underline{\sigma}$.

$$\underline{\varepsilon} = \underline{\varepsilon}^C + \sum \underline{\varepsilon}^J = (C^C + \sum C^J)\,\underline{\sigma} = C^m\,\underline{\sigma} \tag{7}$$

The implicit joint-continuum model simulates complex mechanical behavior for a rock mass with multiple fracture sets, where complicated elastoplastic models emulate behaviors of each fracture set and the intact media.

Implicit joint-continuum model and transverse isotropic model are implemented in the multi-dimensional FEM simulator Geo-COUS (Geo-COUpled Simulator) developed to investigate coupled phenomena in the porous and fractured media subjected to multi-phase flow (Shin and Santamarina, 2017).

2.3. Validation: Elastic Deformation

Consider a column made of a fractured rock with a single fracture set subjected to a stress perturbation in the vertical Z-direction (inset Fig. 2a – Note: U_X and U_Z are the horizontal and vertical displacements at the center of the top plane). The analytical solution for the equivalent elastic modulus E^m (Amadei and Goodman, 1981; Yoshinaka and Yamabe, 1986) and the displacement ratio U_X/U_Z are functions of the fracture dip angles β^J and the fracture stiffness ratio k_r.

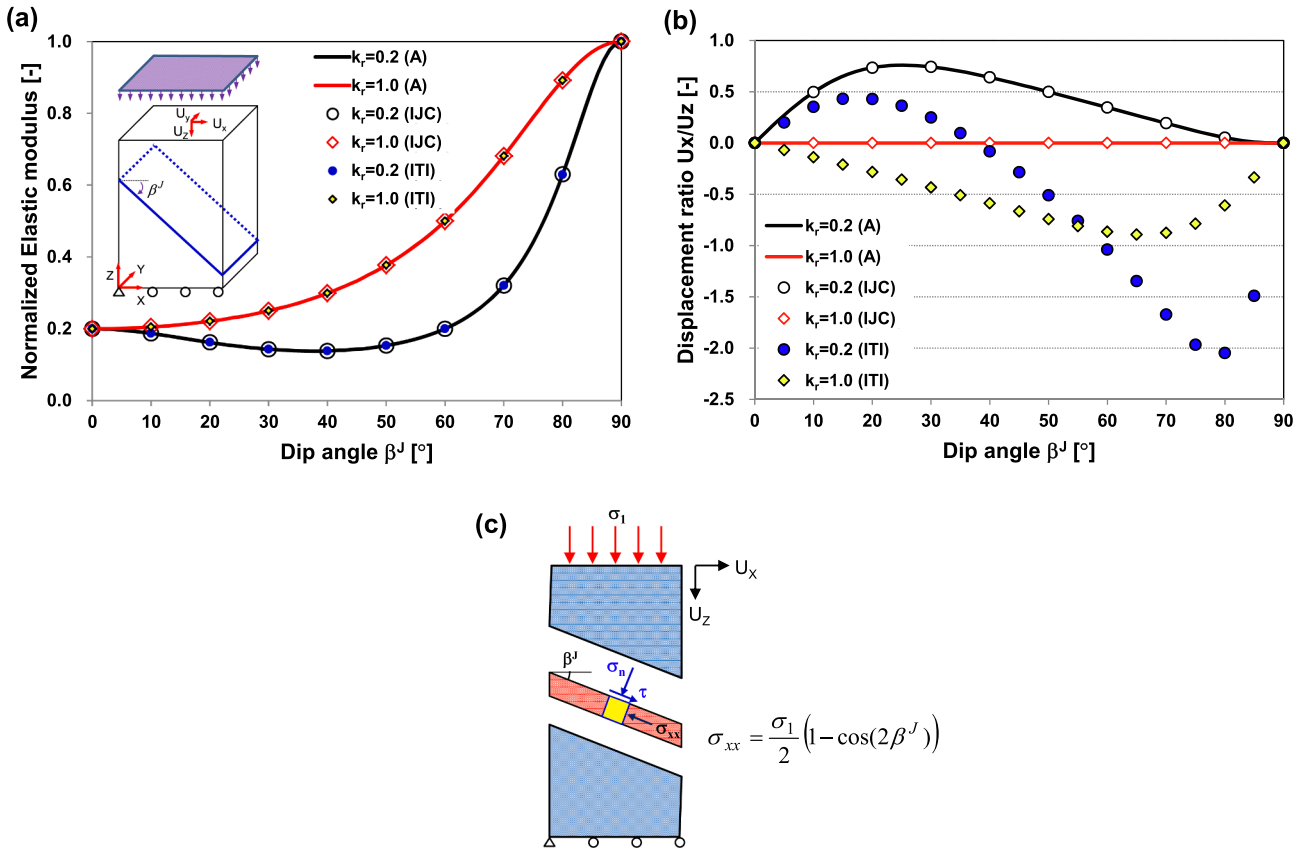

Fig. 2. Deformation of a rock mass with a single joint set under uniaxial compression condition. (a) Variation of normalized stiffness E^m/E^C with dip angle β^J, (b) Variation of horizontal-to-vertical displacement ratio U_X/U_Z with dip angle β^J. (c) Force equilibrium in inclined transverse isotropic model. Analytical solution (A), and numerical solutions for inclined transverse isotropy (ITI) and implicit joint continuum (IJC).

$$\frac{1}{E^m} = \frac{1}{E^C} + \frac{cos^2\beta^J \cdot (cos^2\beta^J + sin^2\beta^J/k_r)}{K_n \cdot s} \tag{8}$$

$$U_X/U_Z = \frac{2sin(2\beta^J) + sin(4\beta^J)}{2sin^2(2\beta^J) + \frac{8k_r(1+K_n \cdot s/E^C - sin^2\beta^J)}{1-k_r}} \tag{9}$$

where E^C is the elastic modulus of the intact rock, and fracture stiffness ratio ($k_r = K_s/K_n$) is shear to normal stiffness ratio for the deformation on the fracture plane. Fig. 2a shows the normalized elastic modulus E^m/E^C for various dip angles β^J (model parameters in Table 1). The analytical solution (Equations (8) and (9)) matches the numerical results computed with both the "inclined transverse isotropic model" and the "implicit joint-continuum model" for the two different fracture stiffness ratios k_r.

In agreement with mechanistic considerations, the analytical solution and the two numerical models show that the displacement ratio is $U_X/U_Z = 0$ for intact rock, for a rock mass with very high fracture stiffness, or for the extreme case of horizontal $\beta^J = 0°$ or vertical fractures $\beta^J = 90°$. However, the U_X/U_Z vs. dip angle β^J trends highlight pronounced differences between the two models (Fig. 2b):

- the analytical solution is in full agreement with numerical simulation results computed with the implicit joint-continuum model.
- the transverse isotropic model predicts very different U_X/U_Z values: it shows negative U_X for fracture dip angles $\beta^J > 40°$ at $k_r = 0.2$ and a full range of dip angles at $k_r = 1.0$. Note that the figure displays U_X/U_Z values computed with the finite element code and using the theoretical solution based on stress and strain rotations – not shown here.

The marked discrepancies in U_X/U_Z predictions in Fig. 2b underline the fundamental differences between these models. The transverse isotropic model requires stress continuity for all stress components through the anisotropic plane and induces bedding-parallel stress (σ_{xx}) to decrease U_X/U_Z (Fig. 2c). This guarantees a positive definite stiffness tensor. On the other hand, the implicit joint-continuum model recognizes that fractures must transfer σ_{zz}, σ_{zx} and σ_{zy} to satisfy equilibrium, but it allows stress discontinuity for σ_{xx}, σ_{yy} (where the z-direction is normal to the fracture plane). The following section explores

Table 1
Material properties in numerical simulation.

	Properties	
Fig. 2	Intact rock	Linear-elasticity: $E^C = 10$GPa, $\nu = 0.3$
	Joint set	Linear-elasticity: $E^C/(s \cdot K_n) = 4.0$. s = 0.5 m, $k_r(=K_s/K_n) =$ 0.2,1.0
Fig. 3	Intact rock	Linear-elasticity: $E^C = 10$GPa, $\nu = 0.25$
	Joint set	Linear-elasticity: $E^C/(s \cdot K_n) = 0.94$, s = 0.5 m, $k_r = 0.067$ (Note: same parameters as the example in Goodman 1989).
Fig. 4	Intact rock	Linear-elasticity: $E^C = 10$GPa, $\nu = 0.25$
	Joint set	Linear-elasticity: $E^C/(s \cdot K_n) = 0.94$, s = 0.5 m, $k_r = 0.067$ Coulomb-plasticity: c^J(cohesion) = 0, ϕ^J(friction angle) = 45°, δ^J(dilation angle) = 30°
Fig. 5	Intact rock	Linear-elasticity: $E^c = 10$ GPa, $\nu = 0.25$
	Joint set	Linear-elasticity: $E^c/(s \cdot K_n) = 0.94$, s = 0.5 m, $k_r = 0.067$ Coulomb-plasticity: c^J(cohesion) = 0, ϕ^J(friction angle) = 45°, δ^J(dilation angle) = 30°
Fig. 6	Intact rock	Linear-elasticity: $E^c = 10$ GPa, $\nu = 0.3$
	Joint set	Linear-elasticity: $E^c/(s \cdot K_n) = 4.0$, s = 0.5 m, $k_r = 0.2$

implications for the case of shallow foundations.

3. Implications: Shallow foundations

This section revisits previous studies and provides new results using the implicit joint-continuum model. Table 1 summarizes the material parameters for the intact rock and fracture sets used in the following studies.

3.1. Line load: Bray's solution

Bray (1977) provides the analytical solution for the radial stress distribution due to a line load normal to the surface of a transverse isotropic half-space as a function of fracture plane orientation β^J, the intact rock to fracture stiffness ratio $E^C/(s{\cdot}K_n)$, and the fracture set shear-to-normal stiffness ratio k_r (Note: Bray's derivation was not published). This highly cited analytical solution predicts severely distorted stress bulbs in fractured rock masses (Duncan and Christopher, 2005; Goodman, 1989; Oda et al., 1993; Singh, 1973) in agreement with experimental results (e.g., block system with two staggered orthogonal fracture sets in Gaziev and Erlikhman, 1971).

Stress distribution from Bray's equation is compared with numerical results from the inclined transverse isotropy and the implicit joint-continuum models. The plain strain finite element model consists of 8-node displacement and 4-node fluid pressure continuum elements (120,801 nodes and 40,000 elements). The plain-strain simulations involve a 100 m wide and 100 m high domain with sliding-displacement boundary on both lateral and bottom. Results summarized in Fig. 3 show:

- The three cases on the left (Fig. 3a) show very good agreement between the radial stress σ_r distribution computed using Bray's equation (white lines) and numerical results computed with the inclined transverse isotropic model (colored bulbs). Numerical results confirm the absence of tangential σ_θ and shear stress $\tau_{r\theta}$ in the entire domain due to the surface line load, in agreement with Bray's assumption (Note the similarity to Flamant's solution for the stress field induced by a line load normal to the surface of an elastic half-space).
- The three plots on the right (Fig. 3b) present the radial stress field computed using the implicit joint-continuum model. Pressure bulbs are very similar to Bray's theoretical solution for fracture dip angles $\beta^J = 0°$ and $\beta^J = 90°$. However, the radial stress field for $\beta^J = 45°$ shows a single stress bulb normal to the fracture set, rather than the two orthogonal stress bulbs predicted by Bray's solution and the transverse isotropic model (see also Bindlish et al., 2012; Agharazi et al., 2012). The radial stress bulb parallel to the dip direction of the joint comes from the continuity of bedding-parallel stress (σ_{xx}) in the transverse isotropic model (see Fig. 2c and Fig. 3a for $\beta^J = 45°$.).

Differences between predictions obtained with the transverse isotropy model and the implicit joint continuum model follow previous observations in Fig. 2. The implicit joint-continuum model allows for stress discontinuity and transfers only stress components acting on the joint plane.

3.2. Strip load on a fractured rock mass

Numerical analysis is performed for the strip footing on the surface of a fractured rock mass with a single fracture set at a dip angle $\beta^J = 60°$. Fig. 4 presents the mean stress field in the rock mass at three load levels.

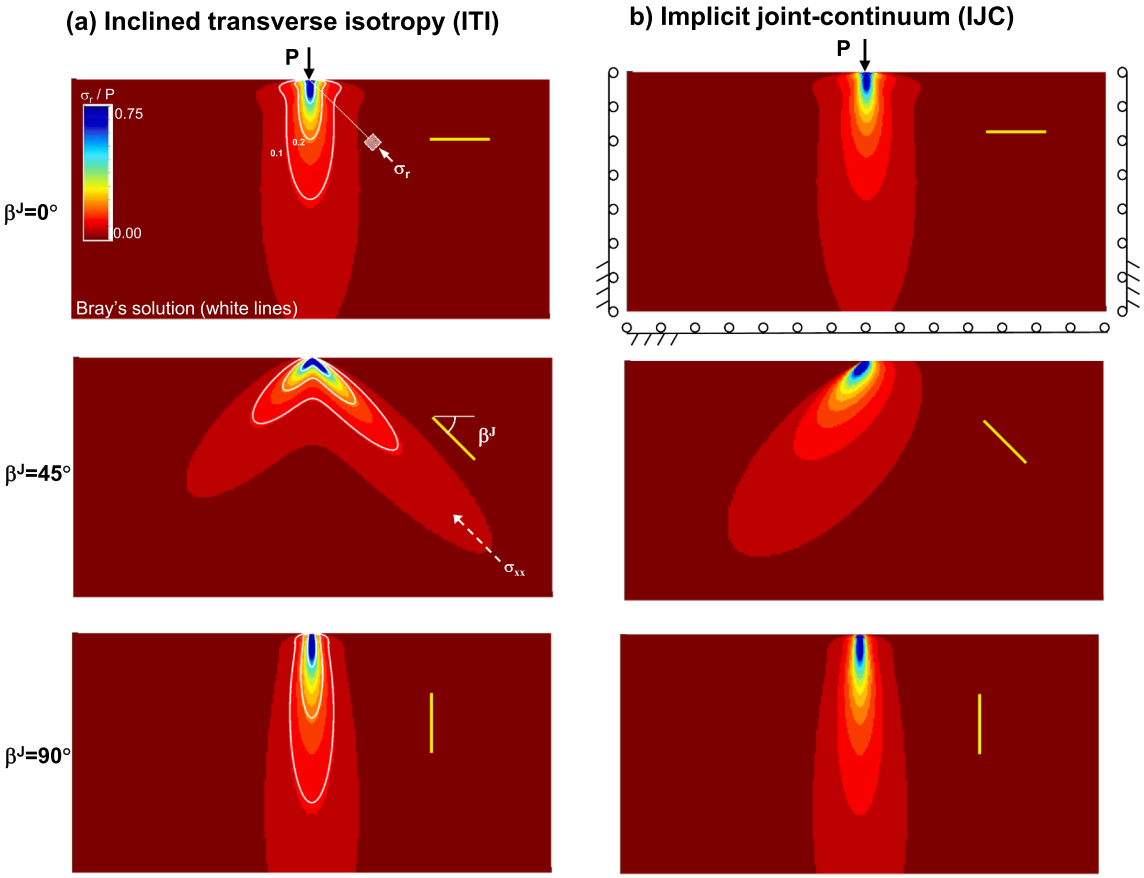

Fig. 3. Radial stress (σ_r) bulb due to line load on the surface of a fractured rock mass with a single fracture set.

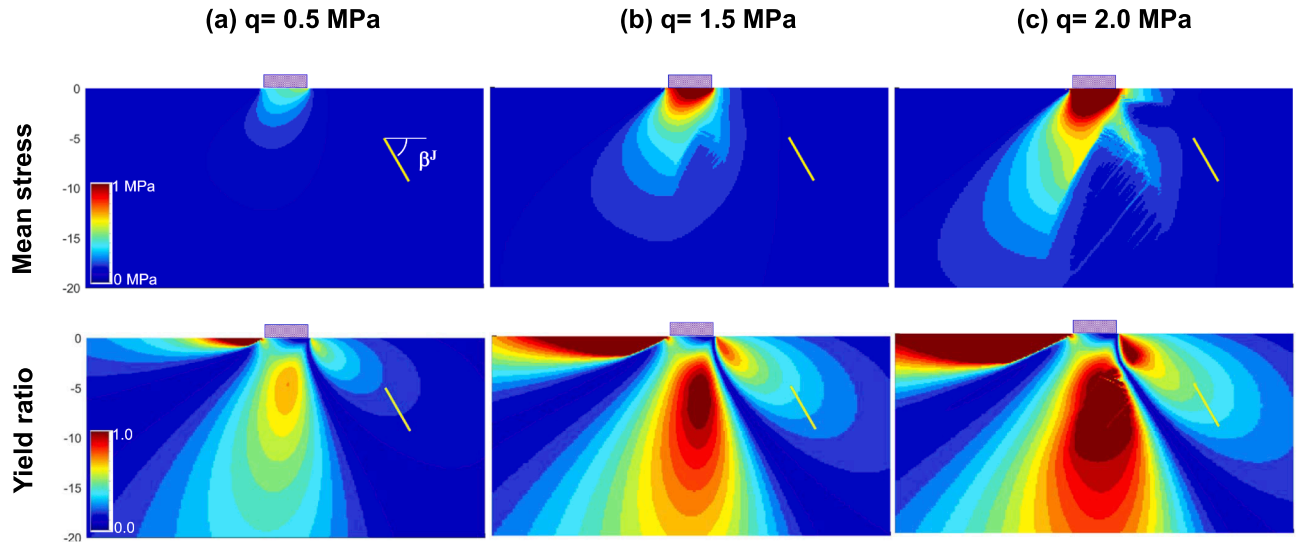

Fig. 4. Distribution of mean stress in the intact rock and yield ratio of the joint due to different strip load (q) on the surface of a fractured rock mass with a single fracture set (dip angle $\beta J = 60°$). Footing width B = 5 m.

The elastic response of the matrix and fractures determines stress contours before fractures reach shear failure (Fig. 4a for $q \leq 1.2$ MPa - Refer to Fig. 3 for the shape of radial stress bulb). Local shear failure is controlled by the shear strength of the fracture set and it gradually skews the stress bulb (Fig. 4b). Eventually, there is a dramatic change in the mean stress field under the footing ($q \geq 2.0$ MPa - Fig. 4c), and the stress bulb narrows parallel to the fracture direction. Yield ratio is the ratio of acting shear stress to shear strength on the fracture plane. The parallel zone to the fracture direction has a lower yielding ratio and still high mean stress level than its surroundings.

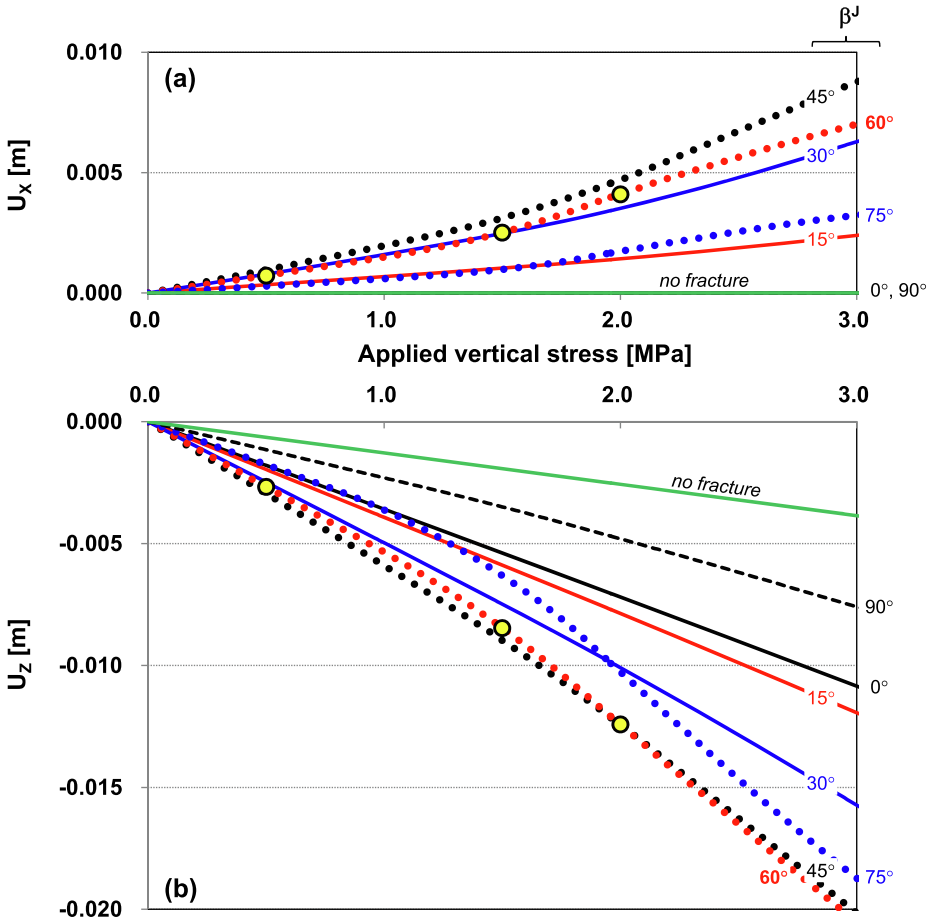

Fig. 5. Strip footing on the surface of a fractured rock mass with a single fracture set. (a) Vertical (U^Z) displacement with various dip angles β^J, (b) Horizontal (U^X) displacement with various dip angles β_J. The yellow dots correspond to the three cases ($\beta^J = 60°$) shown in Fig. 4. (For interpretation of the references to colour in this figure legend, the reader is referred to the web version of this article.)

Fig. 5 shows the horizontal and vertical displacements at the center of the strip footing for different fracture dip angles β^J as a function of the applied load q. These results show:

- There is no horizontal displacement at the center of the footing resting on intact rock or on the rock mass with either horizontal $\beta^J = 0°$ or vertical $\beta^J = 90°$ fractures due to geometrical symmetry and compatibility (Fig. 5a).
- The vertical displacement is greater for the footing on fractured rock than on intact rock (Fig. 5b). The underlying mechanisms depend on the dip angle: the fracture normal stiffness softens the rock mass for $\beta^J = 0°$, but stress focusing and deeper depth of influence are observed along with rock columns beneath the footing for $\beta^J = 90°$. The slight non-linearity observed for $\beta^J = 90°$ results from shear yielding along vertical joints beneath the strip loading.
- Dip angles between $\beta^J = 30°$ and $\beta^J = 75°$ accentuate the non-linear trend between the vertical displacement and the applied load, as the non-linear fracture response has greater impact on the observed boundary deformations.
- The footing load that triggers yielding and the ensuing plastic zone depend on the fracture dip angle.

Simulation results reported in Figs. 4 and 5 correspond to a rock mass made of elastic intact rock and a elasto-plastic single fracture set. Therefore, the load-deformation response does not reach ultimate capacity (Note: the implemented numerical code does incorporate elastoplastic matrix response and multiple fracture sets).

3.3. Effect of fracture strike and dip

Experimental results showed that the modulus of subgrade reaction had a minimum at the dip angle nearby 30° although with an experimental imperfection due to the bottom boundary constraint (Lee and Jeong, 2016), and that the prevailing vertical displacement into the fracture dip direction causes tilting for fracture dip angles $\beta^J = 45°$ (Dvorak, 1966; Gaziev and Erlikhman, 1971; Majumder, 2015).

This section uses the implicit joint-continuum model to investigate the effects of fracture strike and dip on the subgrade stiffness, and the footing displacement and tilt. The problem geometry involves a strip footing (B = 5 m) running in the North-South direction, and resting on a rock mass with a single fracture set (dip angle β^J, strike angle θ^J - See sketch in Fig. 6a). The strip footing problem is inherently plane-strain, therefore it allows for vertical U_Z and horizontal U_X displacements only.

Results for all β^J and θ^J angles can be found in the Supplementary Information associated to this paper, where data are presented on a Lambert azimuthal equal-area projection. For clarity, trends extracted in Fig. 6 show the extreme conditions where fractures are either aligned with the strip footing ($\theta^J = 0°$) or normal to it ($\theta^J = 90°$). The following observations are fully consistent with the complete dataset.

The plots reveal prevalent trends in the subgrade reaction of the rock mass normalized by the intact rock, i.e., the normalized settlement ratio U_Z^r/U_Z^{rm} (Fig. 6b), the horizontal displacement at the center of the foundation normalized by the vertical displacement U_X/U_Z (Fig. 6c), and foundation tilt (Fig. 6d). The three figures have a similar symmetric/antisymetric character with respect to $\theta^J = 0°$ and $\theta^J = 90°$. In particular, the following can be derived:

- *Quasi-vertical fracture set* $\beta^J \to 90°$: the subgrade is stiffest, $U_Z^r/U_Z^{rm} \to 1.0$, the horizontal displacement is $U_X/U_Z \approx 0$ (particularly for fracture sets that strike normal to the strip footing $\theta^J \to 90°$), and tilt vanishes.
- *Quasi-horizontal fracture set* ($\beta^J \to 0°$ or 180°): the subgrade can be quite compressible, but there is minimal horizontal displacement $U_X/U_Z \approx 0$ and tilt.
- *Fracture set strikes quasi-collinear with the strip direction* ($\theta^J < \pm 15°$): the subgrade is the most compressible, $U_Z^r/U_Z^{rm} \to 0.14$, and both the horizontal displacement ratio U_X/U_Z and tilt are maximum when the fracture dip angle is either $\beta^J \approx 35° \pm 10°$ or $\beta^J \approx 145° \pm 10°$:

4. Conclusions

Fractures have a prevalent effect on the mechanical properties of fractured rock masses. Engineering analyses often use the inclined transverse isotropic model because it is simple and allows for efficient

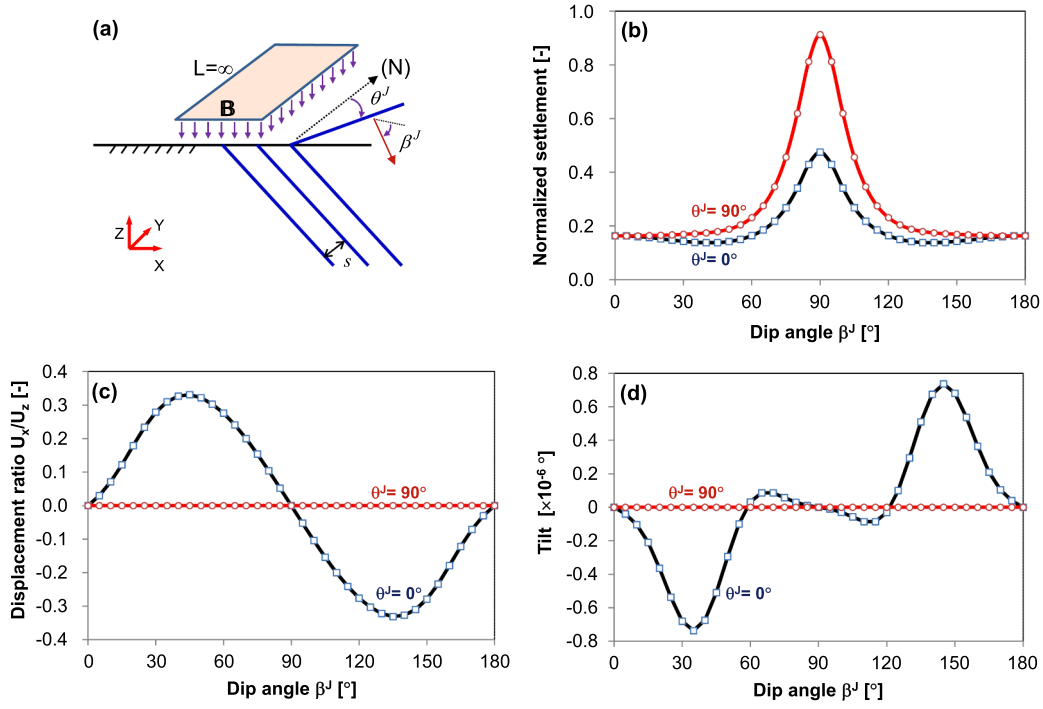

Fig. 6. Strip footing on the surface of a fractured rock mass with a single fracture set with various strike θ^J and dip angle β^J (a) Geometry. (b) Normalized subgrade reaction = settlement U_Z^r/U_Z^{rm}. (c) Displacement ratio U_X/U_Z. (d) Tilt of the footing.

numerical simulations of fractured rock masses in the elastic regime. However, this model is limited to a rock mass with a single fracture set, and it involves inherent assumptions on the continuity for all stress components to guarantee a positive definite stiffness tensor. The inadequacy of transverse isotropy to model fractured rock media becomes apparent in the internal stress distribution and displacement field for various boundary-value problems, such us foundations.

The implicit joint-continuum model combines the mechanical response of the intact rock and the fractures through their compliance matrices. It only allows transferring stress components acting on the normal face of the joint. Numerical simulations with simple boundary-value problems corroborate the numerical implementation against closed-form analytical solutions. The parametric study of strip foundations resting on a fractured rock mass predicts maximum settlement and tilt when the fracture set strikes quasi-collinear with the strip direction ($\theta^J \approx \pm 15^\circ$) and the fracture dip angle is either $\beta^J \approx 40^\circ \pm 10^\circ$ or $\beta^J \approx 140^\circ \pm 10^\circ$.

CRediT authorship contribution statement

Hosung Shin: Conceptualization, Data curation, Formal analysis, Funding acquisition, Investigation, Methodology, Software, Validation, Visualization, Writing - original draft, Writing - review & editing. **J. Carlos Santamarina:** Conceptualization, Investigation, Methodology, Validation, Writing - original draft, Writing - review & editing.

Declaration of Competing Interest

The authors declare that they have no known competing financial interests or personal relationships that could have appeared to influence the work reported in this paper.

Acknowledgements

This research was supported by Research Funds from the National Research Foundation of Korea (KNRF-2019004419) and the KAUST endowment. G. Abelskamp edited the manuscript.

Appendix A. Supplementary material

Supplementary data to this article can be found online at https://doi.org/10.1016/j.compgeo.2021.104317.

References

Agharazi, A., Martin, C.D., Tannant, D.D., 2012. A three-dimensional equivalent continuum constitutive model for fractureed rock masses containing up to three random fracture sets. Geomech. Geoeng. 7 (4), 227–238.
Alehossein, H., Carter, J.P., Booker, J.R., 1992. Finite element analysis of rigid footings on fractureed rock. Proceedings of the Third International Conference on Computational Plasticity 2, 935–945.
Amadei, B., Goodman, R.E., 1981. A 3-D constitutive relation for fractured rock masses. In: Proceedings of the International Symposium on Mechanical Behaviour of Structured Media, pp. 249–268.
Bell, F.G., 1992. Engineering in rock masses. Butterworth-Heinemann, Jordan Hill.
Bieniawski, Z.T., 1973. Engineering classification of fractureed rock masses. Trans. S. African Instn. Civ. Engrs. 15 (12), 335–344.
Bindlish, A., Singh, M., Samadhiya, N.K., 2012. Ultimate bearing capacity of shallow foundations on fractureed rock mass. Indian Geotech. J. 42 (9), 169–178.
Bray, J.W., 1977. Unpublished note. Imperial College, London.
Cai, M., Horii, H., 1992. A constitutive model of highly fractureed rock masses. Mech. Mater. 13 (3), 217–246.
Cho, J.W., Kim, H., Jeon, S., Min, K.B., 2012. Deformation and strength anisotropy of Asan gneiss, Boryeong shale, and Yeoncheon schist. Int. J. Rock Mech. Min. Sci. 50, 158–169.
Davis, E.H., 1980. Note on some plasticity solutions relevant to the bearing capacity of brittle and fissured materials. Proc. Int. Conf. Struct. Found. Rock. 3, 83–90.
Duncan, C.W., Christopher, W.M., 2005. Rock slope engineering-civil and mining, 4th ed. Taylor and Francis.
Dvorak, A., 1966. Tests of anisotropic shales for foundation of large bridges. In: 1st Congress-1966-221 ISRM Conference, pp. 537–541.
Gaziev, E., Erlikhman, S., 1971. Stress and strains in anisotropic foundations. Symp. on Rock Fracture. ISRM (Nancy, paper II-1).
Gerrard, C.M., Harrison, W.J., 1970. Circular loads applied to a cross-anisotropic half space. Technical Paper. CSIRO. 8.
Goodman, R.E., 1989. Introduction to Rock Mechanics. Wiley, New York.
Hudson, J.A., Harrison, J.P., 2000. Engineering rock mechanics - An introduction to the principles. Elsevier.
Hungr, O., Coates, D.F., 1978. Deformability of rock fractures and its relation to rock foundation settlements. Can. Geotech. J. 15, 239–249.
Imani, M., Fahimifar, A., Sharifzadeh, M., 2012. Upper bound solution for the bearing capacity of submerged fractureed rock foundations. Rock Mech. Rock Eng. 45 (4), 639–646.
Jing, L., 2003. A review of techniques, advances and outstanding issues in numerical modelling for rock mechanics and rock engineering. Int. J. Rock Mech. Min. Sci. 40, 283–353.
Lee, J., Jeong, S., 2016. Experimental study of estimating the subgrade reaction modulus on fractureed rock foundations. Rock Mech. Rock Eng. 49 (6), 2055–2064.
Liao, J.J., Wang, C.D., 1998. Elastic solutions for a transversely isotropic half-space subjected to a point load. Int. J. Numer. Analyt. Meth. Geomech. 22 (6), 425–447.
Maghous, S., Bernaud, D., Fréard, J., Garnier, D., 2008. Elastoplastic behaviour of fractureed rock masses as homogenized media and finite element analysis. Int. J. Rock Mech. Min. Sci. 45, 1273–1286.
Majumder, D., 2015. Behaviour of shallow foundation on fractureed rock mass. Indian Institute of Technology Roorkee. Ph.D Thesis.
Oda, M., Yamabe, T., Ishizuka, Y., 1993. Elastic stress and strain in fractureed rock masses by means of crack tensor analysis. Rock Mech. Rock Eng. 26 (2), 89–112.
Prakoso, W.A., Kulhawy, F.H., 2004. Bearing capacity of strip footings on fractureed rock masses. J. Geotech. Geoenviron. Eng. 130 (12), 1347–1349.
Serrano, A., Olalla, C., 1996. Allowable bearing capacity of rock foundations using a non-linear failure criterium. Int. J. Min. Sci. Geomech. Abstr. 33 (4), 327–345.
Shin, H., Santamarina, J.C., 2017. Sediment-well interaction during depressurization. Acta Geotech. 12, 883–895.
Shin, H., Santamarina, J.C., 2019. An implicit joint-continuum model for the hydro-mechanical analysis of fractured rock masses. Int. J. Rock Mech. Min. Sci. 119, 140–148.
Singh, B., 1973. Continuum characterization of fractureed rock masses - Part ii: Significance of low shear modulus. Int. J. Min. Sci. Geomech. Abstr. 10 (4), 337–349.
Sutcliffe, D.J., Yu, H.S., Sloan, S.W., 2003. Lower bound solutions for bearing capacity of fractureed rock. Comput. Geotech. 31 (1), 23–36.
Wang, C.D., Pan, E., Tzeng, C.S., Han, F., Liao, J.J., 2006. Displacements and stresses due to a uniform vertical circular load in an inhomogeneous cross-anisotropic half-space. Int. J. Geomech., ASCE. 6 (1), 1–10.
Yoshinaka, R., Yamabe, T., 1986. Fracture stiffness and the deformation behavior of discontinuous rock. Int. J. Min. Sci. Geomech. Abstr. 23, 19–28.
Yu, H.S., 2006. Plasticity and Geotechnics. Springer.
Zhang, H., Zhu, J., Liu, Y., Xu, B., Wang, X., 2012. Strength properties of fractureed rock masses based on the homogenization method. Acta Mech. Solida Sin. 25 (2), 177–185.
Zhang, Z.M., Lei, W.D. 2014. Influence of intermediate principal stress on correction formula of bearing capacity of rock foundation. Rock Engineering and Rock Mechanics: Structures in and on Rock Masses. Taylor and Francis Group. London. 529-532.